

Coordinated Path-Following for Multi-Agent Fixed-Wing Aircraft

Hugo Sequeira Costa
hugosequeiracosta@tecnico.ulisboa.pt

Instituto Superior Técnico, Universidade de Lisboa, Portugal

October 2021

Abstract

This work addresses the problem of coordinated path-following for fixed-wing Unmanned Aerial Vehicles (UAVs) for a fixed altitude set-point. The problem is partially decoupled by decomposing it first in a path-following sub-problem by commanding the attitude of each UAV, and second in a sub-problem of coordinating their respective along-path parameters by adjusting their speeds about their nominal desired speed profiles. In relation to the path-following problem, two different algorithms are considered. In the first algorithm, the path is decomposed into a concatenation of straight-lines; the controller being linearisation-based. In the second algorithm, a vector field curved path-following controller is considered, whose stability is explored through Lyapunov and input-to-state stability analysis, presenting conditions for which global asymptotic stability of the system may be concluded. With respect to the coordination, a proportional-integral consensus coordination control law is considered, valid for a communication topology with integral connectivity. Simulation results illustrating the functioning of both coordinated path-following algorithms are presented and discussed.

Keywords: coordinated path-following, coordination control, path-following, unmanned aerial vehicles (UAVs), fixed-wing.

1. Introduction

Unmanned Aerial Vehicles (UAVs) have found increasing uses in academic, military, and practical applications, such as in reconnaissance, and surveillance missions. Nevertheless, their restricted capabilities in terms of power, sensing, communication, and computation have generated interest in the use of teams of UAVs to improve the capability, capacity, and flexibility of the Unmanned Aerial System (UAS). Advantages include the ability to parallelise individual tasks, increase the tolerance of the whole system to sensor and hardware failures, and the possibility of giving different capabilities to each UAV [1, 2]. A large subset of these missions require that the UAVs coordinate their motion in relative and/or absolute time [1]. Examples of these cooperative mission scenarios are sequential auto-landing and coordinated ground-target suppression for multiple UAVs [2].

Control of multi-agent systems is a research area experiencing increasing growth [3]. Information interaction is an important concern in multi-agent systems. It depends on the sensing and communication capabilities of each individual agent, which

are subject to a limited range of perception, a limited bandwidth of communication, limited network resources, and other network-induced issues. To model the information exchange among the agents, graph theory is frequently employed by representing the information exchange by either a directed or undirected graph, possibly time-varying. The main areas of research that have been focused on consensus, formation control, and flocking.

The consensus problem studies the problem of reaching agreement on the states of the agents through distributed local interactions between them. Several algorithms exist such as the simple single integrator consensus algorithm [4], the proportional-integral consensus algorithm used in [1, 2], Kalman-consensus [5], passivity-based designs [6–8], and other non-linear algorithm [9, 10].

Cooperative path-following control consists in coordinating each agent the agents to meet desired temporal constraints, while each follows its assigned desired spacial path. The agents coordinate by means of consensus algorithms on variables describing their progress on the path. It essentially extends a path-following controller by adding a con-

sensus coordination mechanism to the system.

Ihle, Arcaç and Fossen [8] develop a passivity approach for coordinate path-following of general non-linear systems by combining a passive path-following control algorithm for each UAV with a passive synchronization algorithm.

Ghabcheloo et al. [11] studied the coordinated path-following, also for non-linear systems, under communication losses and time delays, and derived sufficient conditions for the stability of the system.

Kaminer et al. [1] and Xargay et al. [2] extend and apply this last study to address the problem of steering a fleet of fixed-wing UAVs along desired paths while meeting spatial and temporal constraints. A 3-D path-following control law is used, but the maximum angular rate constraints of each aircraft are not considered.

Chen et al. [12], a coordinated path-following approach is proposed for group leaders. A virtual target along the desired path is assigned for each leader UAV, whose updating law ensures their coordination. The leader UAVs then track their respective virtual target. The maximum turn-rate constraint is taken into account, but only flight at a constant altitude is considered.

Chen et al. [13] presents a hybrid path-following control law for a fixed-altitude set-point. This hybrid approach defines an invariant coordination set for each aircraft in which the aircraft coordinates with the others. Outside this coordination set, the aircraft tracks its own path independently until it enters the coordination set. It considers both the velocity and turn-rate constraints.

Wang, Wang and Zhu [14], a control law for the more general problem of cooperative moving path-following control is provided, with consideration for speed constraints and collision avoidance. It also only considers flight at a constant altitude.

The objective of this work is to investigate the problem of coordinated flight of fixed-wing aircraft at a fixed altitude set-point. For this purpose, the problem is formulated as a coordinated path-following problem, where aircrafts are required to follow desired spacial paths while coordinating on their positions along them to meet desired spacial and temporal constraints. It is assumed that for each aircraft a desired spacial path and a speed profile that solve the required cooperative mission and satisfies the aircrafts' kinematic and dynamic constraints have been assigned. Following the approach of Kaminer et al. [1] and Xargay et al. [2], the problem is partially decoupled by decomposing it first in a path-following sub-problem by commanding the attitude of each UAV, and then coordinating their respective along-path parameters by adjustment of their speeds around their desired speed profiles to ensure the aircrafts keep their de-

sired time separation along the path. For the path-following sub-problem two control laws are considered. First, a linearisation-based control law for paths consisting of a concatenation of straight-line segments. Second, a non-linear vector field curved path-following control law. For the coordination sub-problem, a proportional-integral consensus coordination control law is used.

The subsequent sections in this paper describe and analyse the proposed algorithms to solve each of the sub-problems produced by the decomposition of the coordinated path-following considered. The algorithms are implemented in a simulation environment and their results discussed.

Section 2 focuses on the path-following sub-problem. The control model used for path-following control law design is first described in subsection 2.1, followed by the presentation of the two alternative path-following algorithms considered in the work.

In subsection 2.2, the first path-following algorithm is presented, a linearised path-following controller able to follow paths composed of sequences of straight-line segments. The simple half-plane switching method is chosen to perform the switching between segments, and the controller for each segment is synthesized. The subsection is concluded by describing the conditions required for local asymptotic stability.

In subsection 2.3, the second algorithm is presented, a non-linear vector-field path-following controller capable of following general curved paths. The stability analysis performed in Zhao et al. [15] was found to be incomplete and has been corrected and extended to account for time-varying speeds, presenting conditions for which global asymptotic stability of the system may be concluded.

In section 3, the coordination problem is described, and the chosen coordination algorithm presented. The integration of this algorithm with the path-following algorithms presented in section 2 is described in detail.

Section 4 presents the obtained simulation results of the implementation of the algorithms in a Simulink simulation environment. Based on the results, the control behaviour and performance of the algorithms is analysed and compared.

The work is concluded in section 5 by summarizing the objectives set and the results achieved. It also includes a roadmap for the extension of the work undertaken and suggestions for further investigation.

2. Path-Following

2.1. Mathematical Model

In the following, it is assumed that each aircraft is equipped with an autopilot capable of maintain-

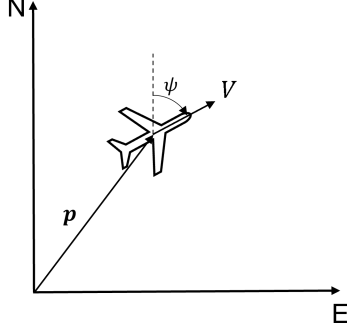


Figure 1: Diagram illustrating the variables of the control model.

ing the desired altitude set-point, and of controlling it in a coordinated turn. In order to simplify the analysis of the following path-following control algorithms, it is also assumed the aircraft flies in no wind. Under these assumptions, the kinematic model for the aircraft is

$$\dot{\mathbf{p}} = \mathbf{R}(\psi)V\mathbf{e}_1 \quad (1)$$

$$\dot{\psi} = \frac{g}{V} \tan \phi, \quad (2)$$

where $\mathbf{p} = (x, y)^T$ is the North-East position of the aircraft in a local inertial reference frame, ψ is the heading of the aircraft,

$$\mathbf{R}(\psi) = \begin{pmatrix} \cos \psi & -\sin \psi \\ \sin \psi & \cos \psi \end{pmatrix} \quad (3)$$

is the rotation matrix from the direction of the speed of the aircraft to the local inertial reference frame, V is the airspeed of the aircraft, $\mathbf{e}_1 = (1, 0)^T$, g is the local acceleration of gravity, ϕ is the roll angle of the aircraft. The airspeed and the roll angle are considered to be the inputs, since it is assumed that the autopilot controls these aircraft variables on a much faster time-scale than the path-following algorithms that will be presented. The geometric variables may be visualized in figure 1.

The roll angle input is transformed to the turn rate command by

$$\omega^c = \frac{g}{V} \tan \phi. \quad (4)$$

Leading to the model that will be considered for the path-following algorithms to be presented

$$\dot{\mathbf{p}} = \mathbf{R}(\psi)V\mathbf{e}_1 \quad (5)$$

$$\dot{\psi} = \omega^c, \quad (6)$$

subject to the kinematic input constraints

$$0 < V_{\min} \leq V \leq V_{\max} \quad (7)$$

$$|\omega^c| \leq \omega_{\max}(V). \quad (8)$$

These constraints are imposed by the flight characteristics of fixed-wing UAVs. In the first constraint, the lower bound is due to the existence of a minimum airspeed under which the aircraft is not capable of maintaining the level flight, the stall speed, and the upper bound is due to the aircrafts maximum thrust capability. The second constraint is imposed by the maximum roll angle that it is to be allowed to the aircraft, where

$$\omega_{\max}(V) = \frac{g}{V} \tan \phi_{\max}. \quad (9)$$

2.2. Linearised Path-Following Controller

This controller works by approximating the desired path for each aircraft by a concatenation of straight-line segments, whose end-points will be denoted by $\{\mathbf{w}_0, \mathbf{w}_1, \dots, \mathbf{w}_N\}$. The transition between the different segments is implemented using the half-plane switching method [16]. In this method, the path controller switches to the next segment when it has crossed the bisecting plane between this and the current segment.

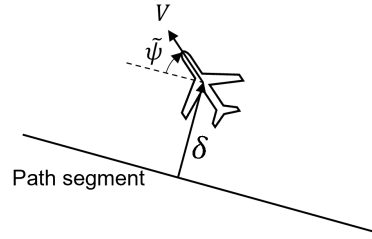


Figure 2: Diagram of the geometric variables of the Linearised Path-Following Controller.

The controller is designed to steer the UAV to the current segment being followed. The objective is to reduce the lateral distance of the UAV to the path to zero. For this purpose, denote the lateral distance to the path by δ , considering it to be positive when the UAV is to the right of the path, negative otherwise. As such, its dynamics are described by

$$\dot{\delta} = V \sin \tilde{\psi}, \quad (10)$$

where $\tilde{\psi} = \psi - \Psi_0 \in]-\pi, \pi[$ is the heading relative to the path's direction (cf. figure 2).

Linearising this last equation around the path heading for a given airspeed V , combining with equation (6), and introducing the integral controller state $\delta_I = \delta + \delta_{aw}$ to ensure asymptotic convergence to the path, produces the linearised system

$$\begin{pmatrix} \dot{\delta}_I \\ \dot{\delta} \\ \dot{\tilde{\psi}} \end{pmatrix} = \begin{pmatrix} 0 & 1 & 0 \\ 0 & 0 & V \\ 0 & 0 & 0 \end{pmatrix} \begin{pmatrix} \delta_I \\ \delta \\ \tilde{\psi} \end{pmatrix} + \begin{pmatrix} 0 \\ 0 \\ 1 \end{pmatrix} \omega^c + \begin{pmatrix} 1 \\ 0 \\ 0 \end{pmatrix} \delta_{aw}. \quad (11)$$

The following PID control law is implemented

$$\omega_\ell^c = -k_{\delta_I} \delta_I - k_\delta \delta - k_{\tilde{\psi}} \tilde{\psi}, \quad (12)$$

but to satisfy the constraint in the turn-rate (8) this command is saturated

$$\omega^c = \text{sat}_{-\omega_{\max}}^{\omega_{\max}} \omega_{\ell}^c, \quad (13)$$

and the back-calculation anti-wind-up solution is implemented by discharging the integral state by the amount

$$\delta_{\text{aw}} = k_{\delta_I, \text{aw}}(\omega_{\ell}^c - \omega^c). \quad (14)$$

2.2.1. Stability Analysis

By application of the Ruth-Hurwitz stability criterion, the linearised closed-loop path-following system for a given constant speed is stable for the choice of gains

$$k_{\tilde{\psi}} > 0, \quad k_{\delta} k_{\tilde{\psi}} > k_{\delta_I}, \quad k_{\delta_I} > 0. \quad (15)$$

Hence, by Lyapunov's indirect method [17, Theorem 4.7], the non-linear closed-loop path-following system is locally asymptotically stable for a given speed, and this choice of gains.

2.3. Vector-Field Curved Path-Following Controller

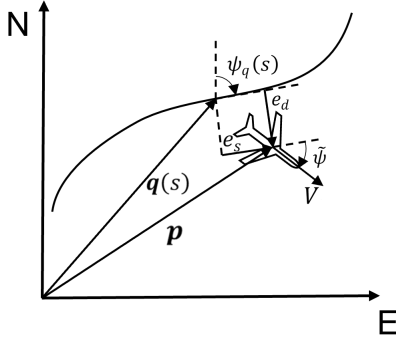


Figure 3: Diagram of the variables used in the Vector-Field Curved Path-Following Controller.

In this method, a non-linear curved path-following controller [15] based on a desired vector field heading is considered. The geometric variables considered are represented in figure 3, where $q: I \subset \mathbb{R} \rightarrow \mathbb{R}^2$ is the parametrization of the path of a given UAV with sectionally continuous second derivative, parametrized by the path-length variable s . A virtual point is introduced on the path, where s is the path-length parameter of the virtual point on the path and $q(s)$ is its position. Define, respectively, the along-track and the cross-track errors as

$$\begin{pmatrix} e_s \\ e_d \end{pmatrix} = R^T(\psi_q(s))(p - q(s)), \quad (16)$$

and the course error as

$$e_\chi = \psi - \psi_q - \tilde{\psi}_d(e_d), \quad (17)$$

where $\psi_q(s)$ is the course angle of the path for the given point parametrized by s , and $\tilde{\psi}_d$ is a desired approach differentiable vector field, function of the cross-track error.

The error system is then described as [15]

$$\dot{e}_s = V \cos(\tilde{\psi}_d(e_d) + e_\chi) - (1 - \kappa(s)e_d)\dot{s}, \quad (18)$$

$$\dot{e}_d = V \sin(\tilde{\psi}_d(e_d) + e_\chi) - \kappa(s)e_s\dot{s}, \quad (19)$$

$$\dot{e}_\chi = \omega - \kappa(s)\dot{s} - \dot{\tilde{\psi}}_d. \quad (20)$$

To make the UAV follow its assigned path by converging the along and cross track errors to zero, the following updating law for the path parameter, control law for the turn rate, and desired approach vector field are chosen [15]

$$\dot{s} = k_s e_s + V \cos \tilde{\psi} \quad (21)$$

$$\omega^c = -k_\omega(e_\chi) + \kappa(s)\dot{s} + \dot{\tilde{\psi}}_d(e_d), \quad (22)$$

and

$$\tilde{\psi}_d(e_d) = -\tilde{\psi}^\infty \tanh(k_d e_d), \quad (23)$$

where $\tilde{\psi}^\infty \in]0, \frac{\pi}{2}[$, $\tilde{\psi} = \psi - \psi_q(s)$, $\kappa(s)$ is the curvature of the path at the point parametrized by s , and k_s , k_d , and k_ω are positive control gains.

2.3.1. Stability Analysis

Proposition 1. *Considering V as a time-varying signal satisfying the bounds in equation (7). Then, system (18)–(19) along with the updating law (21) with state (e_s, e_d) , and input e_χ is regionally input-to-state stable with respect to $\mathbb{R}^2 \times B_r$, with $r = \theta \tilde{\psi}^\infty$, for some $0 < \theta \leq \frac{\pi}{2\tilde{\psi}^\infty} - 1$.*

Proof. The following proof is based on [18, sec. III. D], where the author considers a similar desired course vector-field¹. The main difference being that it uses the geometrically closest point on the path for the determination of the cross-track error. Here the argument is extended for the case being considered where a dynamic update law (21) is used, with the consequent addition of the along-track error and its dynamics (18). In addition, explicit account of the regional character of the input-to-state stability is made, which was absent in the referenced work.

Let

$$V_1 = \frac{1}{2}(e_s^2 + e_d^2). \quad (24)$$

Taking the time derivative,

$$\dot{V}_1 = -k_s e_s^2 + V e_d \sin(\tilde{\psi}_d(e_d) + e_\chi) \quad (25)$$

$$= -k_s(1 - \alpha)e_s^2 + V e_d \sin((1 - \theta)\tilde{\psi}_d(e_d)) \quad (26)$$

$$- \alpha k_s e_s^2$$

$$+ V e_d (\sin(\tilde{\psi}_d(e_d) + e_\chi) - \sin((1 - \theta)\tilde{\psi}_d(e_d))),$$

¹Instead the vector-field being constructed from a hyperbolic tangent, an arc-tangent, multiplied by $\frac{2}{\pi}$ to preserve the geometric meaning of $\tilde{\psi}^\infty$, is used.

for some $\alpha, \theta \in]0, 1[$.

It will be shown that

$$\dot{V}_1 \leq -k_s(1-\alpha)e_s^2 + V_{\min}e_d \sin((1-\theta)\tilde{\psi}_d(e_d)), \quad (27)$$

for $\| (e_s, e_d) \| \geq \rho(|e_\chi|)$, for a class \mathcal{K} function ρ .

The sine function is strictly increasing in the interval $[-\frac{\pi}{2}, \frac{\pi}{2}]$. In this interval,

$$|e_\chi| \leq \theta\tilde{\psi}^\infty \tanh(k_d|e_d|) \quad (28)$$

ensures that the last term in equation (26) is non-positive. Choosing

$$\theta \leq \frac{\pi}{2\tilde{\psi}^\infty} - 1, \quad (29)$$

guaranties that the arguments of the sine lie in the interval, since

$$|\tilde{\psi}_d(e_d) - e_\chi| \leq (1 + \theta)\tilde{\psi}^\infty. \quad (30)$$

Inverting inequality (28),

$$|e_d| \geq \frac{1}{k_d} \operatorname{arctanh}\left(\frac{|e_\chi|}{\theta\tilde{\psi}^\infty}\right). \quad (31)$$

Now assume this last inequality does not hold. Noting that

$$|\sin(\tilde{\psi}_d(e_d) + e_\chi) - \sin((1-\theta)\tilde{\psi}_d(e_d))| \leq 2|e_\chi| + 2, \quad (32)$$

the last term of equation (26) is less than or equal to

$$\frac{2V}{k_d} \operatorname{arctanh}\left(\frac{r}{\theta\tilde{\psi}^\infty}\right) (|e_d| + 1). \quad (33)$$

Thus, if

$$|e_s| \geq \sqrt{\frac{2V}{\alpha k_s k_d} \operatorname{arctanh}\left(\frac{|e_\chi|}{\theta\tilde{\psi}^\infty}\right) (|e_\chi| + 1)}, \quad (34)$$

then inequality (27) is verified.

Noting the bounds (7), defining the class \mathcal{K} function as

$$\begin{aligned} \rho(r) &= \frac{1}{k_d} \operatorname{arctanh}\left(\frac{r}{\theta\tilde{\psi}^\infty}\right) \\ &+ \sqrt{\frac{2V_{\max}}{\alpha k_s k_d} \operatorname{arctanh}\left(\frac{r}{\theta\tilde{\psi}^\infty}\right) (r + 1)}, \end{aligned} \quad (35)$$

achieves the desired result. \square

Proposition 2. *System (20) with the turn rate command control law (22) is globally asymptotically stable, if*

$$|\kappa(s)\dot{s} + \dot{\tilde{\psi}}_d| < \omega_{\max}(V_{\max}). \quad (36)$$

Proof. Let

$$V_\chi = \frac{1}{2}e_\chi^2. \quad (37)$$

Its time derivative subject to control law (22) is

$$\dot{V}_\chi = -k_\omega e_\chi^2, \quad (38)$$

if the turn rate is not saturated.

If it is saturated, then it is equal to

$$\begin{aligned} \dot{V}_\chi &= e_\chi(-\omega_{\max} \operatorname{sgn}(e_\chi) - \kappa(s)\dot{s} - \dot{\tilde{\psi}}_d) \\ &< -\omega_{\max}|e_\chi| + |e_\chi|\omega_{\max} = 0. \end{aligned} \quad (39)$$

Hence [17, Theorem 4.9], the system is globally asymptotically stable. \square

Proposition 3. *System (18)–(20) with control laws (21)–(22) is globally uniformly asymptotically stable if condition (36) is always satisfied.*

Proof. System (18)–(20) is a cascade connection between an input-to-state stable for all states and a subset of the input and a globally asymptotically stable system. Thus, an argument similar to Khalil [17, Lemma 4.7] shows uniform asymptotic stability for any state with $|e_\chi| < \theta\tilde{\psi}^\infty$.

For $|e_\chi| \geq \theta\tilde{\psi}^\infty$, since system (20) with control law (22) is uniformly asymptotically stable, there is a T such that $|e_\chi(T)| < \theta\tilde{\psi}^\infty$. The solution of system (18)–(19) is defined in this interval, so the system progresses to state $(e_s(T), e_d(T), e_\chi(T))$ applying the last argument to this as the initial state yields the desired result. \square

Proposition 4. *For $e_s = 0$, condition (36) is guaranteed to be satisfied if*

$$|\kappa(s)| < \frac{\omega_{\max}(V_{\max})}{V_{\max}} - \tilde{\psi}^\infty k_d. \quad (40)$$

Proof.

$$|\kappa(s)\dot{s} + \dot{\tilde{\psi}}_d| = |\kappa(s)V \cos \tilde{\psi} + V \sin \tilde{\psi} \tilde{\psi}'_d(e_d)| \quad (41)$$

$$\leq V(|\kappa(s)| + \tilde{\psi}^\infty k_d). \quad (42)$$

Thus, having the path curvature satisfy (40) proves the result. \square

3. Coordination Algorithm

The desired path-length of the UAV along its assigned path for time t_d is given by [1]

$$\ell_{d,i}(t_d) = \int_0^{t_d} v_{d,i}(\tau) d\tau, \quad (43)$$

where $v_{d,i}(\tau)$ is the desired speed of UAV i at time τ . Since the desired speed of each fixed wing UAV is strictly positive (equation (7)), this is a strictly increasing function of the desired time t_d , so it is invertible [1]. This inverse function η gives the desired

time that the aircraft should be given the along-path parameter, and shall henceforth be referred to as the UAV's virtual time. For the first path-following algorithm, it is assumed that the speed profile is constant along each path segment. As such,

$$\eta(s) = \frac{\Delta \ell_{i,j}}{v_{d,i,j}} + \sum_{j \in \text{previous segments}} \frac{L_{i,j}}{v_{d,i,j}}, \quad (44)$$

where $L_{i,j}$ is the total length of path segment j of aircraft i , $v_{d,i,j}$ is the desired speed at path segment j of aircraft i , and $\Delta \ell_{i,j}$ is the length the aircraft has covered in the current path segment, given by

$$\Delta \ell_{i,j} = (\cos \Psi_0, \sin \Psi_0)(\mathbf{p} - \mathbf{w}_{i-1}). \quad (45)$$

For second, no restriction is placed on the virtual time beyond the ones for the general case.

The dynamics of each UAV's virtual time are given by

$$\dot{\xi}_i = \frac{\dot{s}_i}{v_{d,i}(\xi_i)}. \quad (46)$$

As a first step, this equation is feedback-linearised. In the case of the first path-following algorithm, the input velocity is transformed by

$$V_{\ell,i} = v_{d,i} u_{\text{coord},i}. \quad (47)$$

For the second one, the transformation is

$$V_i = \frac{-k_s e_{s,i} + v_{d,i} u_{\text{coord},i}}{\cos \tilde{\psi}_i}, \quad (48)$$

valid for $\tilde{\psi}_i \in]-\frac{\pi}{2}, \frac{\pi}{2}[$ (coordination region).

By these transformations, single integrator dynamics are achieved for each of the virtual time coordination states

$$\dot{\xi}_i = u_{\text{coord},i}. \quad (49)$$

The coordination control law implemented for each leader i is [1]

$$u_{\text{coord},i} = -k_P \sum_{j \in \mathcal{N}_i(t)} (\xi_i - \xi_j) + 1, \quad (50)$$

while the one implemented for the followers is

$$\begin{aligned} u_{\text{coord},i} &= -k_P \sum_{j \in \mathcal{N}_i(t)} (\xi_i - \xi_j) + \chi_{I,i}, \\ \dot{\chi}_{I,i} &= -k_I \sum_{j \in \mathcal{N}_i(t)} (\xi_i - \xi_j) \\ &+ k_{\text{coord,aw}}(V - V_{\text{unsat}}), \quad \chi_{I,i}(0) = 1, \end{aligned} \quad (51)$$

where $\mathcal{N}_i(t)$ is the set of neighbours of i at time t , and k_P , $\chi_{I,i}$, and $k_{\text{coord,aw}}$ are positive control gains.

It is assumed that the communication between each UAV is bidirectional and that the information is transmitted continuously with no delays, each vehicle only exchanges its coordination state $\xi_i(t)$ with its neighbours, and the communications graph is connected in an integral sense, i.e., it satisfies the condition

$$\frac{1}{N} \frac{1}{T} \int_t^{t+T} QL(\tau)Q^T d\tau \geq \mu \mathbb{I}_{N-1}, \quad (52)$$

for all $t \geq 0$, where $L(t) \in \mathbb{R}^{N \times N}$ is the Laplacian of the communications graph, Q an $(N-1) \times N$ matrix such that $Q1_N = 0$ and $QQ^T = \mathbb{I}_{N-1}$, 1_N is the vector in \mathbb{R}^n whose components are all 1, and the parameters $T, \mu > 0$ represent the level of connectivity of the communications graph [2].

To ensure the algorithms satisfy the airspeed constraint in equation (7), the speed commands are saturated between these two bounds.

3.1. Coordinated Vector-Field Path-Following Stability

In the case of the coordinated vector-field path-following control, both the path-following and the coordination errors will converge to zero. The path-following control errors converge to zero, since the global asymptotic stability result on the path-following sub-system (subsubsection 2.3.1) is valid for any airspeed satisfying constraint (7).

In regard to the coordination, if any of the aircraft is outside the coordination region, it is unable to coordinate with others by changing its speed. Nonetheless, proposition 2 ensures that each aircraft enters the coordination region in finite time. Then, the coordination states will converge, since the coordination control laws (50) and (51), transformed by (48), with the communication topology satisfying condition (52), are input-to-state stable with the velocity tracking error considered as the input [2, Lemma 3][1, Lemma 4.2].

4. Simulation Results and Discussion

The simulations that will be presented were performed in Simulink, using as the model for each aircraft the kinematic model described by equations (1) and (2).

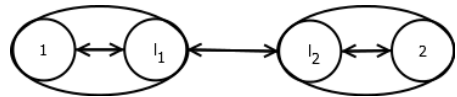


Figure 4: Communication topology. 1 and 2 represent the physical vehicles, while l_1 and l_2 are the virtual leaders.

The chosen communication topology is shown in figure 4. In this topology, each aircraft implements its own virtual leader, with each aircraft communicating its actual virtual time only with its own

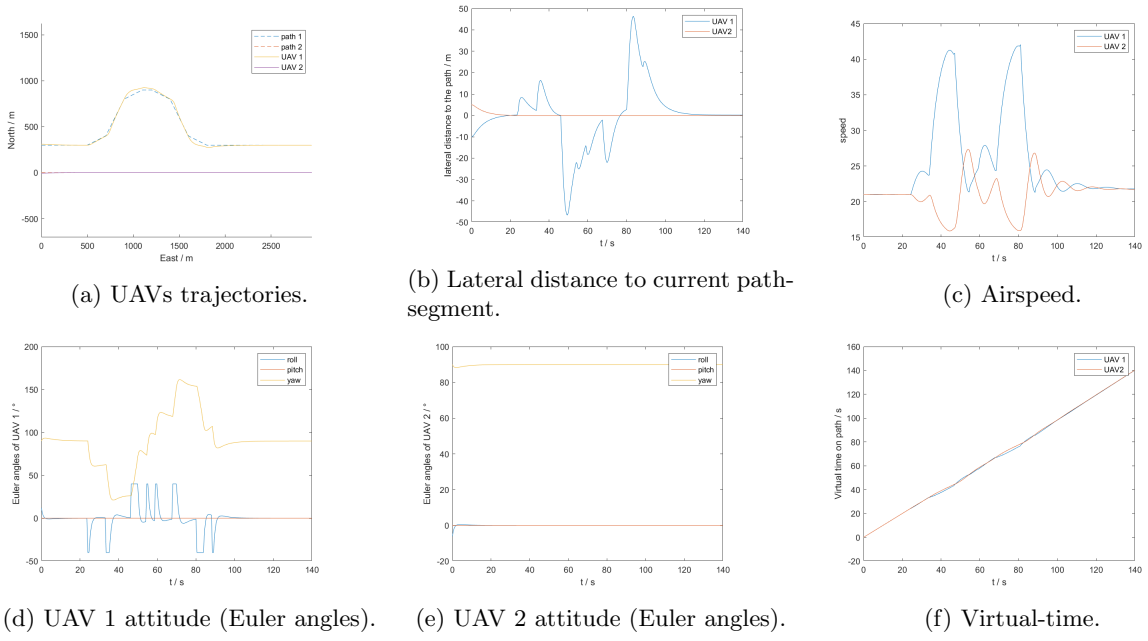


Figure 5: Polygonal detour simulation results (Linearised).

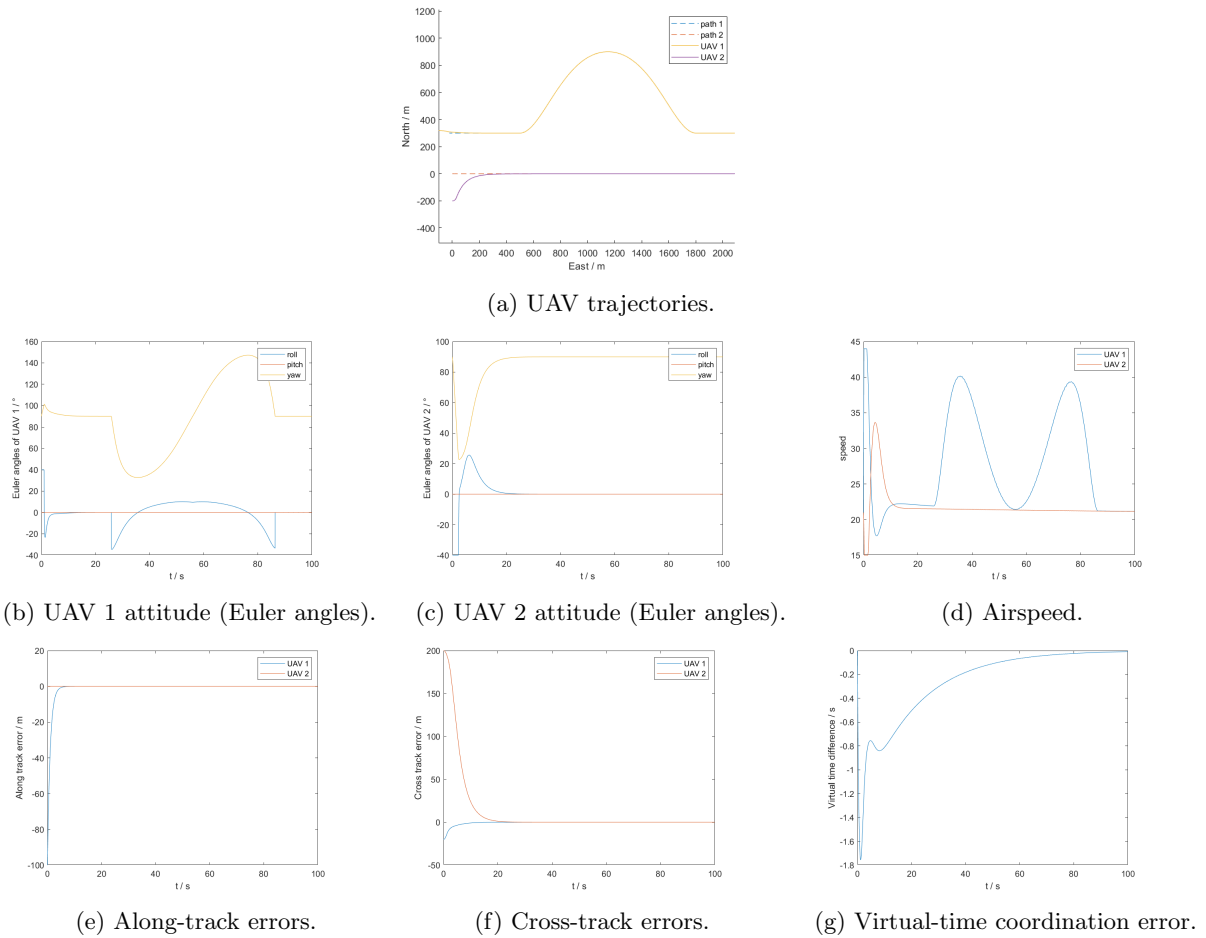


Figure 6: Detour simulation results (Vector-Field).

virtual leader, and the virtual leaders communicating their virtual times between themselves. This addition of virtual leaders with ‘‘uncertainty-free dynamics’’ improves coordination robustness in the presence of disturbances like winds and gusts [1, 19].

Table 1: Model parameters.

g	V_{\min}	V_{\max}	ϕ_{\max}
9.81 m s ⁻²	15 m s ⁻¹	44 m s ⁻¹	40°

Table 2: Path-following controller parameters (Linearised).

k_{δ}	$k_{\tilde{\psi}}$	k_{δ_I}	$k_{\delta_I,aw}$
0.01 m ⁻¹ s ⁻¹	1.4 s ⁻¹	7e-5 m ⁻¹	20 m

Table 3: Path-following controller parameters (Vector-Field).

k_s	k_{ω}	χ^{∞}	k_d
1 s ⁻¹	10 s ⁻¹	70 °	0.01 m ⁻¹

The results of the simulation of the linearised path-following controller are shown in figure 5. In this scenario, the mission is designed so that UAV 1 is required to make a detour (e.g., to circumvent an obstacle) while attempting to remain on the side of UAV 2, who continues on a straight line. It may be seen in figure 5b, that UAV 1 has several spikes in its lateral distance, due to the discontinuity introduced by the chosen segment switching method. This, in turn, leads to significant variations in the speed command seen in figure 5c. Nonetheless, the vehicle is able to converge to its path, even though the roll set-point is always saturated upon each switch, and the vehicles finish the simulation with vehicle 1 behind 2 by only 2 meters. These effects introduced by the discontinuity of the transition may be mitigated by changing the switching algorithm to a smoother one such as a fillet transition [16].

Simulation results for the vector-field curved path-following controller are shown in figure 6. The mission is identical to the former, with the detour being described by two cubic spline segments. UAV 1 starts behind UAV 2, but it may be seen that are able to coordinate and finish the simulation alongside each other with similar speeds, while also converging to their respective paths. Compared to the former algorithm, UAV 1 tracks its path more precisely, and the speed command and roll set-point are smoother.

Table 4: Coordination control parameters.

Algorithm	k_P	k_I	$k_{\text{coord,aw}}$
Linearised	0.9 s ⁻¹	0.03 s ⁻²	0.02 m ⁻¹ s ²
Vector-Field	2 s ⁻¹	0.1 s ⁻²	2 m ⁻¹ s ²

Table 5: Initial conditions (Linearised).

\mathbf{p}_1	$\psi_{0,1}$	\mathbf{p}_2	$\psi_{0,2}$
(310, 0, 0) ^T m	90°	(-5, 0, 0) ^T m	90°

Table 6: Initial conditions (Vector-Field).

\mathbf{p}_1	$\psi_{0,1}$	\mathbf{p}_2	$\psi_{0,2}$
(310, 0, 0) ^T m	90°	(-5, 0, 0) ^T m	90°

5. Conclusions

This work explored the problem of coordinated path-following for fixed-wing aircraft for a fixed altitude set-point by utilizing the framework of coordinated path-following. More specifically, the problem was partially decoupled by decomposing it first in an individual path-following problem by means of the attitude control of each aircraft (section 2), and then a coordination problem of their along-path parameters by adjustment of their speeds around their nominal desired speed profiles (section 3).

Two path-following approaches capable of being integrated into the considered framework were considered in section 2. The first, a path-following controller for a straight-line path was synthesized (section 2.2). Its application was extended to paths consisting of sequences of straight-line segments by the use of the half-plane switching method. Its stability was studied, being concluded local asymptotic stability by the application of Lyapunov’s indirect method (subsection 2.2.1).

The second path-following controller, capable of following general curved paths by means of a desired course vector-field, was described (subsection 2.3). The shortcomings of the stability analysis performed in [15] were corrected and extended to account for time-varying speeds, presenting conditions for which global asymptotic stability of the system may be concluded (subsubsection 2.3.1).

In section 3, each of the path-following control laws were integrated with proportional-integral consensus coordination law from [1, 2], used to coordinate the aircraft relatively on their desired time along their respective path (virtual time) was presented. For each of the previous path-following approaches a coordination map was defined from the along-path-length to the virtual time, and the dynamics of the virtual-time transformed into the canonical single integrator dynamics to which the coordination law may be applied. In addition, the over-

all stability of the cooperative vector-field path-following control law was discussed (subsection 3.1).

The two methods developed in this work were implemented in a Simulink simulation environment, and the results of their simulations were then analysed and compared (section 4). The results illustrate that the non-linear algorithm performs better than the linearisation-based, since it tracks the path more precisely, and is able to achieve the coordination of the aircraft using smoother velocity commands and roll set-points for each of the vehicles.

5.1. Future Work

The analysis of the non-linear curved path-following algorithm in subsection 2.3 should be further analysed in an attempt to prove that for a sufficiently small initial along-track error, it remains small in order to be able to guarantee asymptotical stability for any path that satisfies the curvature constraint (40). Although it seems intuitive that, given the path-parameter updating law (21), the along-track error is at least bounded for small initial values, a detailed analytical proof of this fact was not able to be confirmed.

Flight testing these cooperative path-following solutions, the next step would be to test these algorithms in simulation with the complete model of an aircraft and an inner-loop autopilot capable of tracking the commands of these cooperative path-following solutions.

In order to keep the complexity of the path-following algorithms within the scope of this work, the influence of the wind on the analysis was not considered. This, however, is an important direction of research for future work. In this respect, the use of the integral state in the linearised path-following controller allows for some degree of rejection of wind disturbances, but in the case of the vector-field curved path-following controller, the presence of wind leads to a steady-state path-following error. According to Zhao et al. [15], to compensate the effect of the wind, the airspeed and heading used in the control law could be substituted by the estimated ground-speed, and estimated course, respectively, by means of the wind triangle. To achieve this a wind estimator would have to be integrated, whose combined stability together with the path-following controller would have to be studied. This analysis would be challenged further by the need to satisfy the kinematic input constraints (7) and (8).

Alternatively, 3-D path-following control laws could be explored, such as the ones developed in Brezoescu et al. [20], Liu, McAree and Chen [21] and Yang et al. [22].

In regard to the time-coordination, there are other algorithms that could be explored such as

the Kalman-consensus [5], or other non-linear algorithms [9, 10]. Additionally, a closer consideration to the questions of communication delays and losses could be undertaken.

References

- [1] Isaac Kaminer et al. *Time-Critical Cooperative Control of Autonomous Air Vehicles*. Cambridge, MA: Elsevier, 2017. ISBN: 978-0-12-809946-9. DOI: 10.1016/C2015-0-06603-5.
- [2] E. Xargay et al. ‘Time-Critical Cooperative Path Following of Multiple Unmanned Aerial Vehicles over Time-Varying Networks’. In: *Journal of Guidance, Control, and Dynamics* 36.2 (Mar.–Apr. 2013), pp. 499–516. DOI: 10.2514/1.56538.
- [3] Peng Shi and Bing Yan. ‘A Survey on Intelligent Control for Multiagent Systems’. In: *IEEE Transactions on Systems, Man, and Cybernetics: Systems* 51.1 (Jan. 2021), pp. 161–175. DOI: 10.1109/TSMC.2020.3042823.
- [4] Reza Olfati-Saber, J. Alex Fax and Richard M. Murray. ‘Consensus and Cooperation in Networked Multi-Agent Systems’. In: *Proceedings of the IEEE* 95.1 (Jan. 2007), pp. 215–233. DOI: 10.1109/JPROC.2006.887293.
- [5] Derek B. Kingston, Wei Ren and Randal W. Beard. ‘Consensus Algorithms Are Input-to-State Stable’. In: *Proceedings of the 2005, American Control Conference, 2005*. Vol. 3. 8th–10th June 2005, pp. 1686–1690. DOI: 10.1109/ACC.2005.1470210.
- [6] E. Bıyık and M. Arcak. ‘Passivity-Based Agreement Protocols: Continuous-Time and Sampled-Data Designs’. In: *Group Coordination and Cooperative Control*. Ed. by K. Y. Pettersen, J. T. Gravdahl and H. Nijmeijer. Vol. 336. Lecture Notes in Control and Information Science. Berlin, Heidelberg: Springer, 2006. ISBN: 978-3-540-33469-9. DOI: 10.1007/11505532_2.
- [7] Murat Arcak. ‘Passivity as a Design Tool for Group Coordination’. In: *IEEE Transactions on Automatic Control* 52.8 (Aug. 2007), pp. 1380–1390. DOI: 10.1109/TAC.2007.902733.
- [8] Ivar-André F. Ihle, Murat Arcak and Thor I. Fossen. ‘Passivity-based designs for synchronized path-following’. In: *Automatica* 43.9 (Sept. 2007), pp. 1508–1518. DOI: 10.1016/j.automatica.2007.02.018.

- [9] Hao Chen et al. ‘Consensus in Networks of Nonlinear Integrators with Applications to Coordinated Path Following Control of Fixed-Wing UAVs’. In: *2020 59th IEEE Conference on Decision and Control (CDC)*. 14th–18th Dec. 2020, pp. 5348–5353. DOI: 10.1109/CDC42340.2020.9304199.
- [10] Hao Chen et al. ‘Convergence Analysis of Signed Nonlinear Networks’. In: *IEEE Transactions on Control of Network Systems* 7.1 (Mar. 2020), pp. 189–200. DOI: 10.1109/TCNS.2019.2913550.
- [11] R. Ghabcheloo et al. ‘Coordinated Path-Following in the Presence of Communication Losses and Time Delays’. In: *SIAM Journal on Control and Optimization* 48.1 (11th Feb. 2009), pp. 234–265. DOI: 10.1137/060678993.
- [12] Hao Chen et al. ‘Formation Flight of Fixed-Wing UAV Swarms: A Group-Based Hierarchical Approach’. In: *Chinese Journal of Aeronautics* 34.2 (Feb. 2020), pp. 504–515. DOI: 10.1016/j.cja.2020.03.006.
- [13] Hao Chen et al. ‘Coordinated Path-Following Control of Fixed-Wing Unmanned Aerial Vehicles’. In: *IEEE Transactions on Systems, Man, and Cybernetics: Systems* (2021). DOI: 10.1109/TSMC.2021.3049681.
- [14] Yuanzhe Wang, Danwei Wang and Senqiang Zhu. ‘Cooperative Moving Path Following for Multiple Fixed-Wing Unmanned Aerial Vehicles with Speed Constraints’. In: *Automatica* 100 (Feb. 2019), pp. 82–89. DOI: 10.1016/j.automatica.2018.11.004.
- [15] Shulong Zhao et al. ‘Integrating Vector Field Approach and Input-to-State Stability Curved Path Following for Unmanned Aerial Vehicles’. In: *IEEE Transactions on Systems, Man, and Cybernetics: Systems* 50.8 (Aug. 2020), pp. 2897–2904. DOI: 10.1109/TSMC.2018.2839840.
- [16] Randal W. Beard and Timothy W. McLain. *Small Unmanned Aircraft. Theory and Practice*. Princeton, N.J: Princeton University Press, 2012. ISBN: 978-0-691-14921-9.
- [17] Hassan K. Khalil. *Nonlinear Systems*. 3rd ed. Always Learning. Upper Saddle River, N.J.: Prentice Hall, 2002. ISBN: 0130673897.
- [18] Stephen R. Griffiths. ‘Vector Field Approach for Curved Path Following for Miniature Aerial Vehicles’. In: *AIAA Guidance, Navigation, and Control Conference and Exhibit*. Keystone, Colorado, 21st–24th Aug. 2006. DOI: 10.2514/6.2006-6467.
- [19] Enric Xargay et al. ‘Convergence of a PI Coordination Protocol in Networks with Switching Topology and Quantized Measurements’. In: *51st IEEE Conference on Decision and Control*. Maui, HI, 10th–13th Dec. 2012, pp. 6107–6112. DOI: 10.1109/CDC.2012.6426392.
- [20] A. Brezoescu et al. ‘Adaptive Trajectory Following for a Fixed-Wing UAV in Presence of Crosswind’. In: *Journal of Intelligent & Robotic Systems* 69 (2013), pp. 257–271. DOI: 10.1007/s10846-012-9756-8.
- [21] Cunjia Liu, Owen McAree and Wen-Hua Chen. ‘Path-Following Control for Small Fixed-Wing Unmanned Aerial Vehicles under Wind Disturbances’. In: *International Journal of Robust and Nonlinear Control* 23.15 (7th July 2012), pp. 1682–1698. DOI: 10.1002/rnc.2938.
- [22] Jun Yang et al. ‘Optimal Path Following for Small Fixed-Wing UAVs Under Wind Disturbances’. In: *IEEE Transactions on Control Systems Technology* 29.3 (May 2021), pp. 996–1008. DOI: 10.1109/TCST.2020.2980727.